The International Journal of Advanced Manufacturing Technology (2019) 104:2377–2388
https://doi.org/10.1007/s00170-019-04097-z

ORIGINAL ARTICLE

Experimental analysis of the flow drill screw driving process

Fadik Aslan[1] · Laurent Langlois[2] · Tudor Balan[2]

Received: 15 May 2019 / Accepted: 30 June 2019 / Published online: 5 July 2019

Abstract
Flow drill screw (FDS) driving is a thermomechanical assembly process that allows for single-sided access multi-material joining, with a high application potential for modern lightweight vehicle design. The process combines three consecutive operations which partially overlap: flow drilling, thread forming, and tightening. The paper extensively investigates the process parameter effects on the flow drilling operation of thin sheet AA5182-O 2.5-mm thick and DP600 1.4-mm thick. Drilling defects have been associated with specific ranges of control parameters. Mechanical tests have shown that the drilling defects do not have a significant impact on the mechanical strength of the assembly under static loading. These results were used to determine both the optimal joining parameters and the robust process window. The variation of all process-relevant mechanical quantities was recorded over the whole available process window. This data may further serve for process simulation validation, or alternatively for the construction of data-driven meta-models.

Keywords Flow drilling · Aluminum alloy · AHSS steel · Joining by forming

1 Introduction

Mass reduction has long been identified as a key priority for reducing the CO_2 emissions of vehicles. Modern automobile design focuses on lightweight mixed material construction. Multi-material vehicle design uses lightweight materials such as aluminum alloys combined with high strength steels, as mentioned, for example, by Martinsen et al. [1]. Conventional thermal assembly processes like resistance spot welding are strongly limited for such multi-material joining, because of thermal and metallurgical incompatibility. Meschut et al. [2] recently reviewed a number of alternative innovative joining technologies for multi-material lightweight car body structures, most of which involve plastic deformation of one or both components to be assembled. In addition, automobile structure geometries are becoming more and more complex. For example, extruded tubular components provide only single-sided access for the joining process, further limiting the range of acceptable solutions.

Flow drill screw driving (FDS) is a thermomechanical assembly process used to perform overlay joining with single-sided access. This technology is already used to join dissimilar materials in the premium automotive industry. The FDS process combines three operations, flow drilling, thread forming, and tightening, into a single procedure. A self-drilling and self-tapping screw is used as both tool and fastener. Figure 1 illustrates the FDS process for an overlay joining between two materials (with a pre-hole for the upper component). The first step corresponds to the hole forming in the metal plate. At the start of the process, material is gradually heated thanks to the high rotation speed and axial force applied. The heated metal flows up and down along the screw tip and forms a hole with a bushing, as described by Miller et al. [3]. Then, the second operation of thread forming by plastic deformation starts. During this second stage, the internal thread is formed by deformation of the workpiece material, as demonstrated by Fromentin et al. [4]. In the last operation of the FDS, the screw head approaches the top of the upper component. A final tightening torque is applied in order to ensure a permanent connection. The whole process usually takes between 1.5 and 4.0 s, depending on the material and thickness combination.

✉ Laurent Langlois
laurent.langlois@ensam.eu

Fadik Aslan
fadik.aslan@irt-m2p.fr

Tudor Balan
tudor.balan@ensam.eu

[1] Arts et Métiers ParisTech LCFC, IRT-M2P and Université de Lorraine, 4, Rue Augustin Fresnel, 57070 Metz, France

[2] Arts et Métiers ParisTech LCFC, Université de Lorraine, 4, Rue Augustin Fresnel, 57070 Metz, France

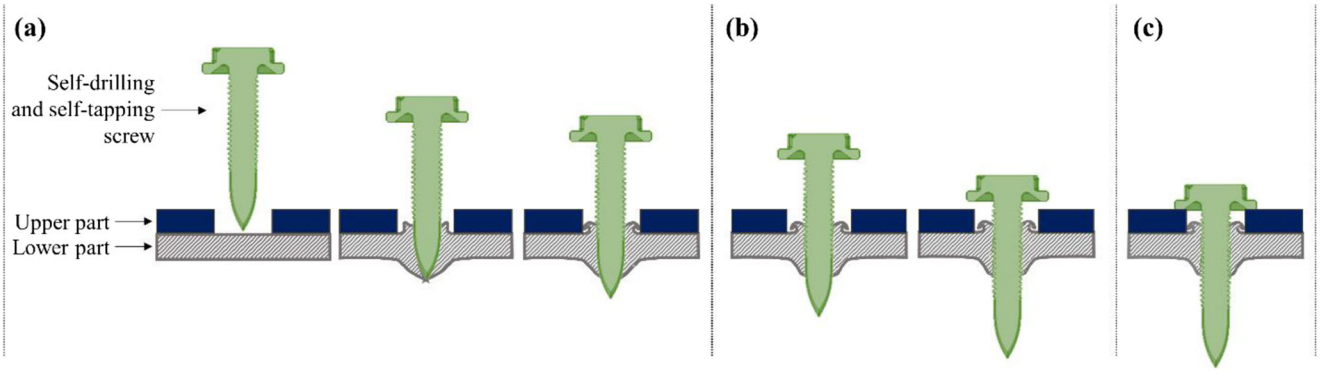

Fig. 1 Illustration of the process stages in flow drill screw driving: (**a**) heating, penetration, and bush forming; (**b**) thread forming and screw advancing; (**c**) tightening

FDS is a joining process recently introduced into the automotive industry. Therefore, research publications on the FDS process are limited. This process is a complex joining technology because of the combination of three operations. Urbikain et al. [5] show that the combination of these successive operations requires adaptation of the process parameters for each step. According to Skovron et al. [6], the major difficulty of this process is to identify the adapted process parameters to obtain a good joint quality.

The flow drilling operation allows the formation of the hole in the work-piece. This step takes the major part of the cycle time of the joining process. Therefore, it is the most important sequence of the FDS process. During flow drilling, the material is subjected to close contact with the screw tip. The work material simultaneously undergoes a temperature increase and significant plastic strain. These two phenomena are mainly controlled by the friction conditions. Streppel et al. [7] note that this operation requires a high contact pressure to generate local heating by friction energy dissipation, because of the small contact surface and short process time required. There is no simple relationship between the process parameters and the generated temperature, because of the strong interactions between temperature, friction, and plastic deformation. This strong interaction is typical also for other friction-based joining processes, e.g., friction stir welding [8] or processes involving intensive plastic strain [9].

Miller et al. [10] suggest that pre-heating the work material and high-speed rotation allow the generation of a cylindrical-shaped bushing. Nevertheless, despite a strong increase in rotation speed (3000 to 15000 rpm), only a small improvement of the bushing formation is observed. The materials used by Miller et al. [10], namely, AI380 and MgAZ91D, have a low maximum elongation (about 3%). As a result, these two materials do not clearly allow for a correlation between the hole quality and the process parameters. The authors further show a reduction in thrust force and torque for high rotation speed, ranging from 3000 to 15000 rpm. Lee et al. [11] also show a thrust force reduction for higher rotation speed for AISI304 stainless steel. However, the authors observe an increase of thrust torque for higher rotation speed, from 3600 to 6000 rpm, regardless of the tool coating. Thus, the two experimental investigations do not show the same trend about the process parameter effect. Miller et al. [12] establish an analytical model to predict the force and torque depending on the tool geometry. They assume a uniform feed speed and neglect the work-hardening effect. The friction is considered of Coulomb type with a constant value. Qu et al. [13] further develop the same type of model by considering a non-deformable contact surface. Reasonable predictions are obtained for the friction coefficient and the shear stress. This approach is limited by the strong assumptions on the friction law and coefficient. In addition, a constant feed rate is assumed in these calculations, whereas an FDS fastener is inserted at a constant force with variable feed rate. Consequently, no direct comparison can be made between the model and the experimental process. For the FDS process, the local heat generated during the flow drilling step is studied by Skovron et al. [14]. For a 6000 rpm rotation speed, the authors show that the generated temperature decreased when increasing the force. Skovron and Miller's work shows similar trends. However, these two works did not make a direct connection between the process parameters and the quality of the formed hole.

Chow et al. [15] show that the parameters defining the tool geometry (friction angle and friction contact areas) have an influence on the hole surface roughness. Friction conditions are often associated with surface roughness. The experimental study of Lee et al. [11] reveals that the hole surface roughness is also related to the tool coating. In flow drilling, it is essential to understand the effect of process parameters on the joint quality. However, research publications on the flow drilling process show that the process parameters are strongly conditioned by the tool–workpiece interface. In the FDS process, a self-drilling screw is used as the drilling tool. The self-drilling screws have major differences compared to conventional flow drilling tools. The material used for self-drilling screws is usually hardened mild steel, according to Sønstabø et al. [16]. Consequently, self-drilling screws are significantly less resistant than conventional

flow drill tools, which are usually made of tungsten carbide. Anti-corrosion coating is compulsory on self-drilling screws, while the flow drill tools are coated with specific anti-wear coatings, as shown by Kerkhofsa et al. [17]. In addition, drilling defects are not directly associated with the drilling parameters in the literature.

The present work proposes a process-effect analysis of the flow drilling step for the FDS process. The correlations between process parameters were investigated, along with their effect on the resulting joint during the flow drilling step. An experimental study was conducted on the effect of rotation speed and feed force on the quality of the formed hole. Based on previous works on the flow drill process, experiments were carried out on a single sheet metal layer with a commercially available self-drilling and self-tapping FDS® screw. Fixing the coating and the screw geometry allows the tool–material interface to be simplified. However, two different work materials were used: sheet aluminum alloy 5182-O and sheet Dual Phase steel DP600. In a first step, the use of these materials made it possible to identify bushing defects and failure modes during the drilling operation. The defects and failure modes were represented in a control chart showing the defect distribution according to the process control parameters (rotation speed and feed force). In a second step, a statistical model was used to describe the dependency of the process time, torque, energy, and energy rate with respect to the process control parameters. The mechanical strength of the FDS joints was tested for several sets of drilling parameters leading to different defects, in order to understand the impact of the flow drilling step on the FDS joining quality.

2 Experimental methodology

2.1 Material

The materials used for the drilling experiments were sheet aluminum-magnesium alloy AA5182-O with a thickness of 2.5 mm and sheet Dual Phase steel DP600 with a thickness of 1.4 mm. These materials are widely applied in the automotive industry. Table 1 shows the average values of strength, hardness, and elongation to failure of the tested materials.

The aluminum–magnesium alloy has a better ductility than the DP600 steel, as shown in Fig. 2. The strength of the aluminum alloy is much less than that of the tool material. These conditions are optimal for obtaining an extensive and complete process control chart. On the other hand, the DP600 steel has a lower ductility and significantly lower thermal conductivity and specific heat than the aluminum. Also, its mechanical resistance approaches that of the tool. These are critical conditions for the flow drill test and made it possible to explore the current challenges of the process.

2.2 Screw and screw driving system

A hole forming and self-tapping screw patented by Grossberndt et al. [18] as FDS® was used, with a reference diameter of 5 mm. This screw has a tip section with 4 lobes and a length of 9.2 mm. The key dimensions and the geometry of this screw are shown in Fig. 3. The screw material is a through-hardened AISI 1018 steel. The FDS® screw is zinc flake coated to provide good protection against corrosion.

A robot-assisted screw driving system RSF21® Weber® was used for the flow drilling experiments, as described by Aslan et al. [19]. The machine used is able to apply a maximum rotational speed of 5000 rpm and a maximum feed force of 3.0 kN. During the FDS process, this machine continuously measures the torque, axial position, feed force, and rotation angle. The machine is able to monitor and stop testing thanks to its automated screw driving system.

2.3 Flow drilling tests

The flow drill test consisted in performing a hole by plastic deformation into a metal plate using the screw tip as a flow drill tool. The work-piece with dimensions 125 × 38 mm was clamped by two screw locking systems on a rigid support with a 30 mm diameter hole, as shown in Fig. 4. The flow drill operation starts with a first contact between the screw tip and the work-piece. The screw is pushed against the plate with a low feed force (300 N). Contact is detected by a decrease of the feed speed when the screw touches the upper surface of the sheet. This operation also ensures a correct alignment of the screw through the guiding socket of the screw driving system. This first contact served to define the reference zero-point for the measurement of the screw position. The drilling rotation speed and feed force were subsequently applied once the screw tip was in contact with the top surface of the work-piece.

Table 1 Thermomechanical properties of the sheet DP600 and AA5182-O. The tensile strength, elongation to failure, and the hardness represent the average value from three tests. The conductivity and specific heat are values provided by the material suppliers

Material	Thickness (mm)	Tensile strength, R_m (MPa)	Maximum elongation (%)	Hardness (HV)	Conductivity [W m^{-1} K^{-1}]	Specific heat [J kg^{-1} K^{-1}]
AA5182-O	2.5	282	25	75	129	902
DP600	1.4	601	17	240	42	447

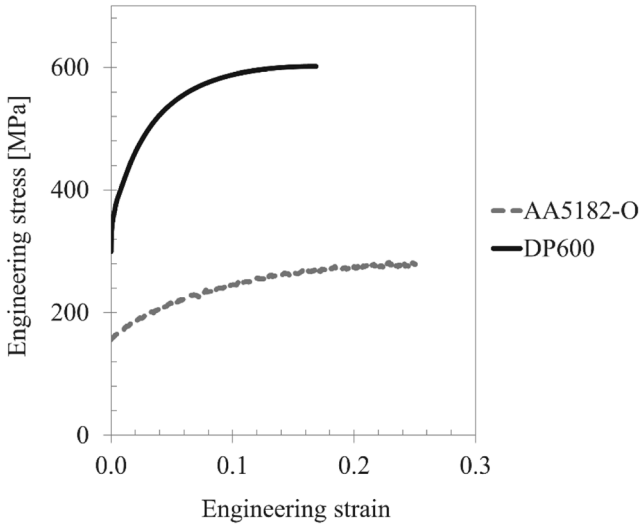

Fig. 2 Representative stress–strain curves up to diffuse necking, at room temperature and low strain rate, for the sheet DP600 and aluminum alloy 5182-O

For the flow drilling test, the process control parameters are the rotation speed and the feed force. Constant values for these two parameters are imposed during the entire drilling step. At the beginning, due to the use of a pneumatic system, a ramp-up time of 0.15 s is necessary to reach the set constant value. This value is kept stable, though not entirely constant, by the pneumatic system. The variation of the process parameters is illustrated in Fig. 5 for a typical drilling test. The flow drilling sequence was stopped when the screw feed position exceeded the pre-set value of 5 mm. The rotation speed, feed force, screw position, torque, angle, and cycle time were measured for all trials, by using the sensors of the screw driving machine RSF21®.

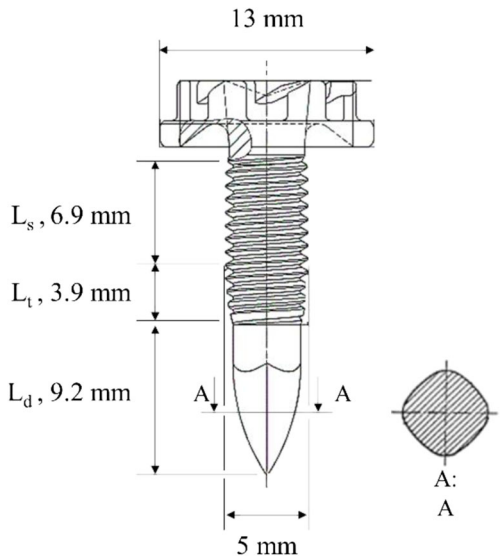

Fig. 3 Key dimensions of the EJOT® FDS® screw, where L_d is the hole forming part length, L_t the thread forming part length, and L_s the usable thread length

The deformation of the aluminum sheet during the flow drilling is illustrated in Fig. 6. The metal sheet progressively deformed around the screw tip. At the beginning of the flow drilling test, between points S1 and S3, the tip penetration in the work-material was done at an almost constant feed speed. The torque and displacement increased almost linearly. Then, the rate of increase of the feed speed and torque was significantly accelerated when the screw displacement exceeded 3 mm. The feed speed value changed, and the screw moved faster until the end of drilling. Following each drilling test, the final geometry of the bushing and the burr (Fig. 6) was analyzed. Macroscopic defects were identified by the final shape of the drilled hole.

2.4 Mechanical joint characterization test

The mechanical characterization test was done in order to control the impact of the drilling parameters on the mechanical performance of the joints. Static tests were carried out with KS-II U-shaped specimens. The specimen dimensions are shown in Fig. 7. This specific test sample is generally used to control the strength of mechanical (FDS, riveting…) and thermal (spot welding) assemblies, as suggested by Szlosarek et al. [20]. This quasi-static test can be done under various loading angles (0°, 30°, 45°, 60°, and 90°). In the present work, the loading angle of 90° representing a pure tensile loading and the loading angle 0° representing a pure shear loading test were used.

The FDS joints were made between the upper part (AA5182-O 2.5 mm) with a pre-hole and the lower part (AA5182-O 2.5 mm), as shown in Fig. 8. For these assemblies, the FDS® screw was used (Fig. 3). Two types of FDS joints were tested. The first assembly series was performed with the drilling parameters corresponding to a uniform bushing. The second case of assembly was done with a crack defect. The parameters used to make these assemblies are presented in Table 2. These two FDS joints differ only in the flow drilling process control parameters.

3 Results

3.1 Process chart and macroscopic defects

Flow drilling control charts are developed to link the process parameters and the macroscopic defects. Jawahir et al. [21] used the machining process control chart to understand the impact of the process parameters on the chip breaking performances of different tools. For the welding process, this kind of chart is also used to show the weldability of a given material couple, as developed by Kim et al. [22]. The application to the FDS process revealed distinct zones in the process parameter space characterized by the occurrence of specific defects. Two

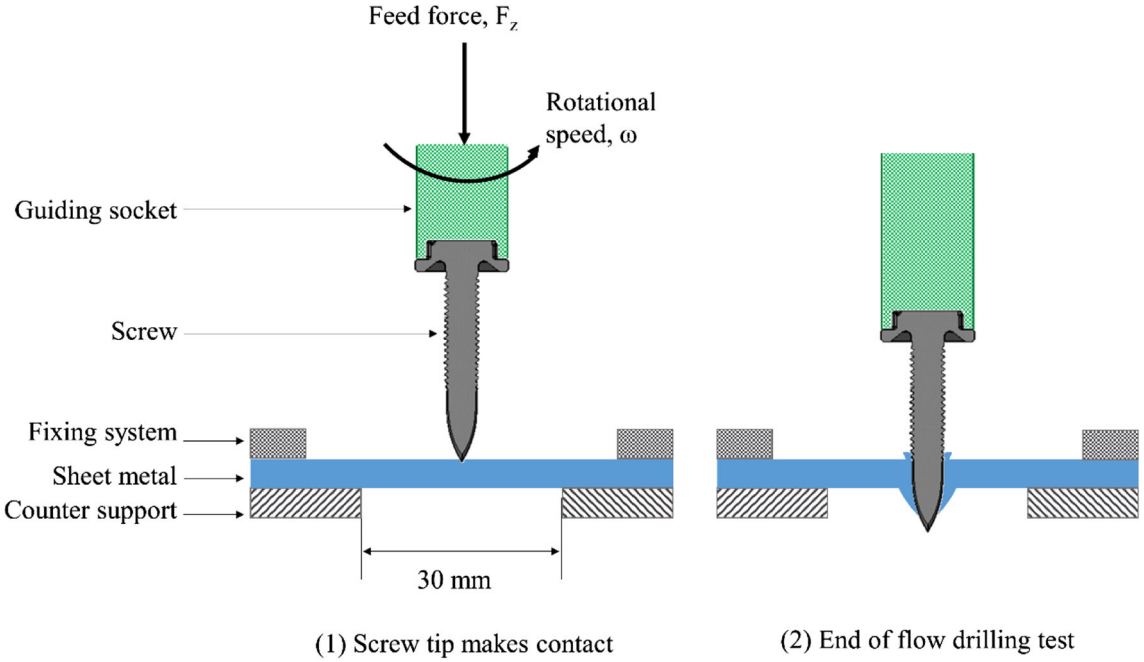

Fig. 4 Illustration of flow drilling test on single-layer sheet metal clamped on a support

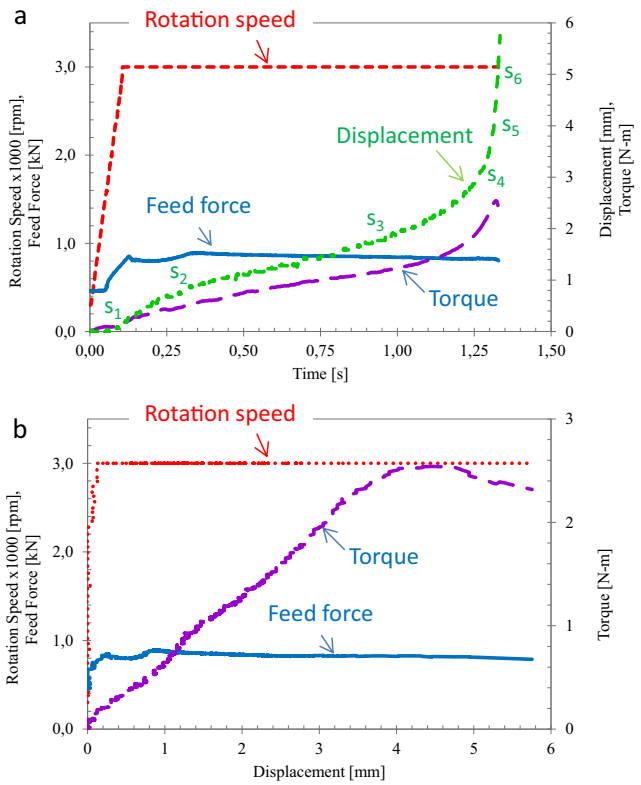

Fig. 5 Variation of flow drill process parameters: rotation speed, feed force (input driving parameters), axial screw displacement, and torque (output parameters) during the flow drilling of an aluminum alloy sample, a. as function of the displacement and b. as function of time. The six points indicated on the displacement curve (S_1…S_6) correspond to the macrographs shown in Fig. 6

control charts were established for the AA5182-O 2.5 mm and DP600 1.4 mm, respectively, and are shown in Fig. 9.

The control chart of the AA5182-O shows that for feed forces greater than 600 N, the material was successfully drilled in all cases. However, the geometry of the resulting bushing and burr depended on the parameter combination. Thus, three zones could be further distinguished, as illustrated by Fig. 10:

- Chips were generated at the upper surface for combinations of high rotation speed and low feed force (Fig. 10b). The formation of chips becomes transitory with the modifications of the control parameters (Fig. 10a, c). In this transition zone, the chip length decreases;
- Deep and irregular cracks occurred at the bottom of the bushing for low rotation speed and high feed force (Fig. 10h). The area representing this defect also presents transient shapes, as illustrated by Fig. 10g, i;
- A uniform ring formed corresponding to a regular bushing and burr (Fig. 10d, e, f). Material flowed upward and downward uniformly with no (or few) cracks or chips. The area identified as “uniform bushing” presents a flawless appearance.

The frontiers between the three zones are not abrupt, as illustrated by cases a, c and g, i, respectively. It is noteworthy that both control charts in Fig. 9 cover the full range of control parameter values allowed by the selected screw driving machine (up to 5000 rpm and 3 kN). Indeed, for the sheet aluminum alloy, feed force values up to 3 kN were set,

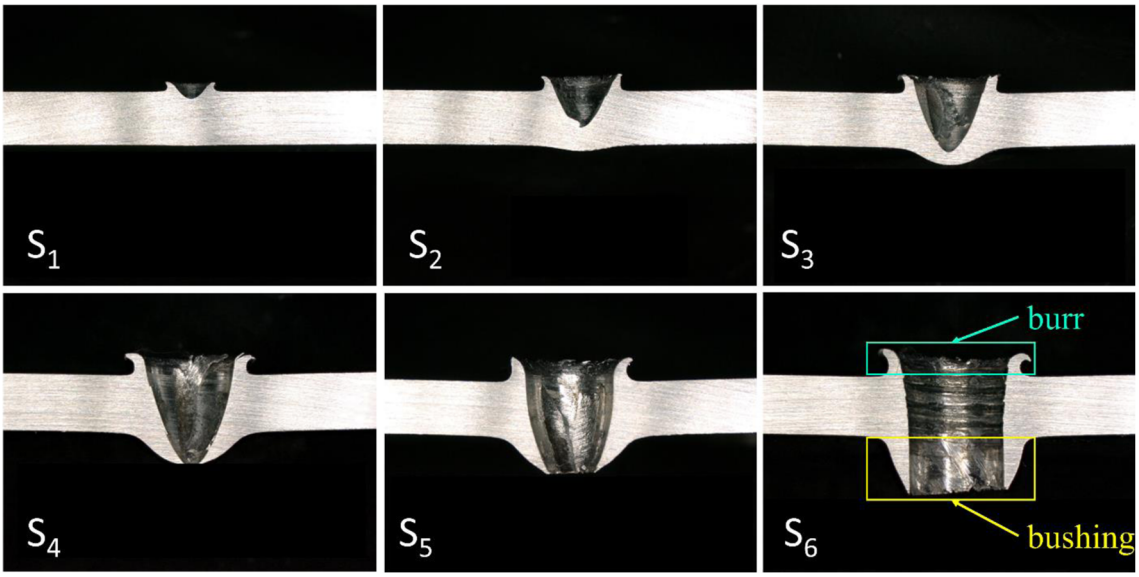

Fig. 6 Illustration of hole geometry forming during the flow drill stage of the 2.5 mm aluminum alloy 5182-O. The resulting samples were cut along the axial plane and polished

although these force levels could never be reached experimentally because of the reduced strength of the material. Thus the right-hand side of the control chart for aluminum does not reach the machine's capacity.

The control chart of the DP600 sheet steel exhibits some similarities, but also striking differences, with respect to the previous one. The cracks in the lower bushing similarly occur for combinations of large feed force and low rotation speed (Fig. 11b). The zone boundaries are similar, except that significantly larger feed forces can be applied with the DP steel. This defect tends to disappear when the feed force is reduced (Fig. 11a), also similarly to the aluminum alloy. One could speculate that the rest of the control chart would also be similar to that of AA5182, although shifted towards larger feed forces. However, the process was significantly limited by the failure of the screw, which trimmed out a very large portion of the potential process parameter control space, which was not reachable by the process. Two screw failure modes were observed, either by torsion shearing (Fig. 11d) or by collapse and buckling (Fig. 11c). As a consequence, the zone allowing for feasible processing without macroscopic defects was very small, although it exists.

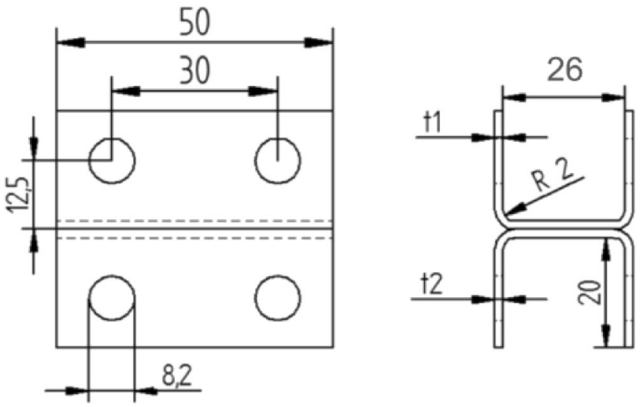

Fig. 7 U-shaped aluminum KS-II test specimen of the Laboratory for Materials and Joining Technology, University of Paderborn

3.2 Process time and torque measurements

During all the experiments, the drilling time and torque were also measured. Each experiment was performed at least three times in order to assess the repeatability of all the measurements. The output parameters were analyzed at 3 mm and 5 mm screw displacement. The torque and displacement measurements were fairly stable up to 3 mm. However, a larger dispersion was observed by the end of the drilling operation. Nevertheless, the measurement at 5 mm is important because these values are very close to the maximum torque value that the screw will undergo during the flow drilling operation.

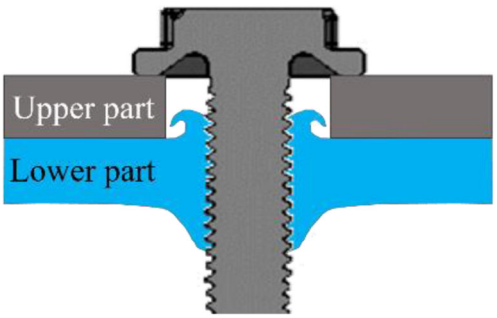

Fig. 8 Illustration of FDS joining with a pre-holed upper part

Table 2 Joint control parameters (drilling, thread forming, and tightening) used to carry out FDS joint with (a) uniform bushing and (b) crack forming defect

	Flow drilling		Thread forming		Tightening		
	Rotation (rpm)	Force (kN)	Rotation (rpm)	Force (kN)	Rotation (rpm)	Force (kN)	Limit torque (Nm)
(a) FDS joint—uniform bushing	5000	1.6	500	0.5	100	0.3	8
(b) FDS joint—crack defect	1500	1.8	500	0.5	100	0.3	8

The results are shown in Fig. 12 for the AA5182-O aluminum alloy, since it exhibits a much larger range of acceptable combinations of rotational speed and feed forces compared to DP600. The results are plotted for three rotation speed values covering the whole range of the process space. The evolutions of the penetration times at penetration depths of 3 and 5 mm are similar, and their values are very close in all cases. The process time significantly increases for lower force values. It tends towards a minimum value when the force increases. The process time also decreases when the rotation speed increases. The two control parameters play an important role in the variation of the time required for penetration and drilling. It is noteworthy that these trends stand for all the zones in the control chart where the drilling is feasible: all the experimental points in Fig. 9a are used, starting from a feed force of 0.8 kN.

The general trend for torque values is an increase with the force and a decrease with the rotation speed (see Fig. 9b). This trend is valid for both screw positions, at 3 mm and 5 mm. However, the torque amplitude is significantly different according to the rotation speed.

3.3 FDS connection mechanical behavior under static loading

Two FDS connections were characterized by means of the KS-II quasi-static test. The assembled U-shaped parts were tested in the loading directions 0° (pure shear) and 90° (pure tensile). Figure 13 shows the results obtained.

For the KS-II-90°, the force–displacement curves are repeatable and similar regardless of the drilling defect. The force increased until approximately 5.7 kN for the FDS connection with a uniform bushing and 5.9 kN for the FDS connection with a crack defect. The maximum force was slightly greater (about 5%) for the FDS connection with the crack defect. The failure mode observed for both connections is the internal threads stripped from the bottom plate, as described by Sønstabø et al. [23]. The sensitivity of the results to the presence or not of cracks can be explained by the fact that the orientation of the cracks is not prejudicial considering the tensile orientation. Moreover, during the tensile test, the cracks can act as blades tightening around the screw increasing by this way the tensile strength of the connection.

For the second loading mode corresponding to a shear stress, the results obtained for the FDS joint with a uniform bushing present one non-repeatable force–displacement curve. The force increased until approximately 9.1 kN for the FDS connection with a uniform bushing and 9.5 kN for the FDS connection with a crack defect. This loading angle shows also that the drilling defect does not significantly affect the mechanical strength of the assembly. The difference in displacement may come from the fact that a cracked bushing allows a higher inclination of the screw during the shear test, as illustrated by the post-mortem appearance of the samples

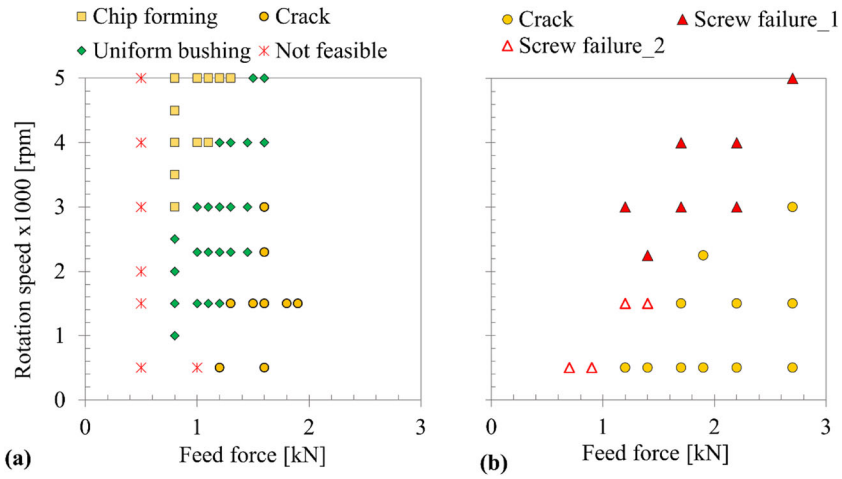

Fig. 9 Control chart of the flow drilling for (**a**) aluminum alloy AA5182-O 2.5 mm and (**b**) DP600 steel 1.4 mm

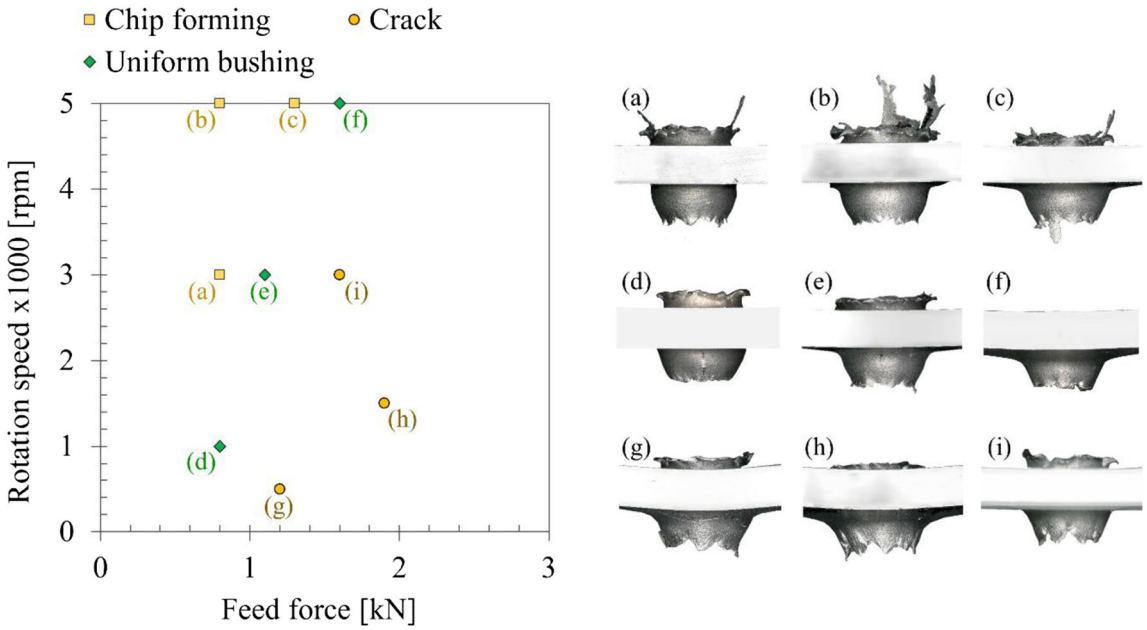

Fig. 10 Three types of drilling bushing shapes for AA5182-O: (**d**, **e**, **f**) uniform bushing; (**a**, **b**, **c**) chip forming; (**g**, **h**, **i**) crack forming. (**a**, **c**) Intermediate shapes with incipient chip forming; (**i**, **g**) intermediate shapes with incipient crack forming

(Fig. 13e, f). The better orientation of the screw according to the shear direction probably explains the better resistance of the connection when the formed bush exhibits cracks.

4 Discussion and data analysis

Process defects like cracks and chips were associated with specific combinations of process parameter values. The occurrence of bushing cracks was probably due to a lack of ductility of the material during drilling, as proposed by Miller et al. [10]. It is certainly a consequence of the combination of the material temperature in the drill zone and the feed force. Nevertheless, the presence of the observed defects did not penalize the process and the joint performance, at least under static loading. As a consequence, the process parameters may be selected within wider ranges, in order to optimize other industrially relevant criteria. From the process viewpoint, the major efficiency criteria are the process cycle time, the maximum torque, the energy consumed, and the maximum power required. During the experiments, the torque was continuously measured as a function of time until the end of the drilling

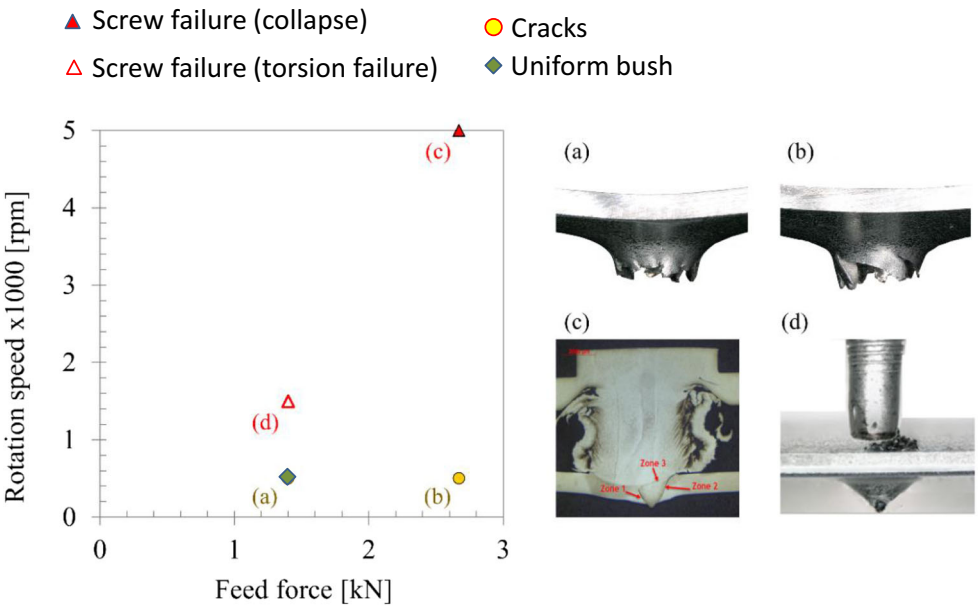

Fig. 11 Two bushing shapes for DP600: (**a**) uniform bushing; (**b**) crack forming. Two screw failures: (**c**) collapse, (**d**) torsion failure, designated "screw failure 1" and "screw failure 2," respectively, in Fig. 9b

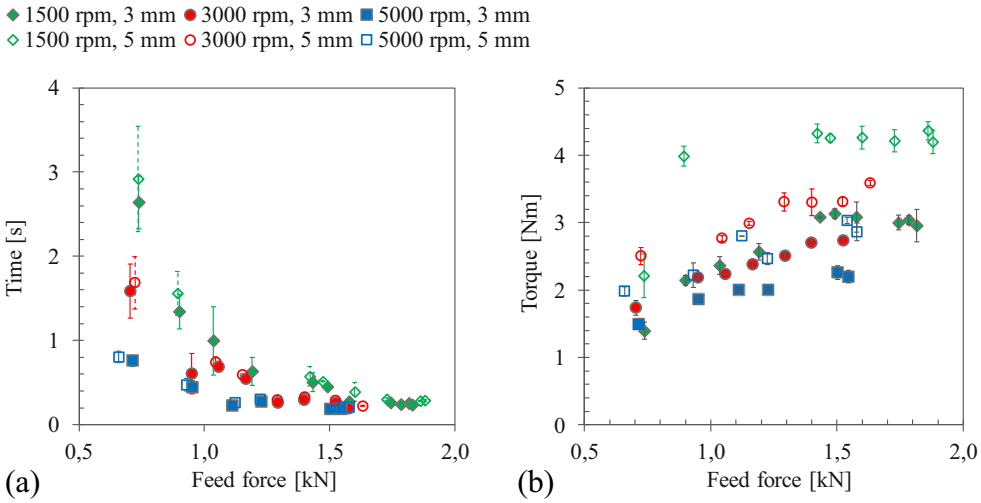

Fig. 12 Time and torque variation according to the feed force for three ranges of rotation speed at the end of penetration (at 3 mm) and at the end of drilling (at 5 mm). The tested material is the sheet aluminum alloy 5182-O

stage, along with the screw stroke. From these measurements, the consumed energy E and work rate P could be directly evaluated as

$$E = \int_0^{\Delta t} M\omega.dt + \int_0^{\Delta t} F_Z v.dt, \quad (1)$$

$$P = M\omega + F_Z v, \quad (2)$$

where Δt is the time duration of drilling, F_Z the feed force, v the tool axial velocity, t the time, M the torque, and ω the tool rotational speed. According to the recorded data, the contribution of the feed force to the power and the energy was negligible; thus, both power and energy were solely associated with the tool rotation and torque.

In order to further exploit the available experiments, a simple power law was used to interpolate the experimental values over the entire domain:

$$X(F_z, \omega) = a_0 F_Z^{a_1} \omega^{a_2}, \quad (3)$$

where X designates the interpolated quantity, and a_0, a_1, and a_2 are the parameters of the interpolation law. This law gave very good results for the interpolation of process time and energy. The torque and power required a more flexible

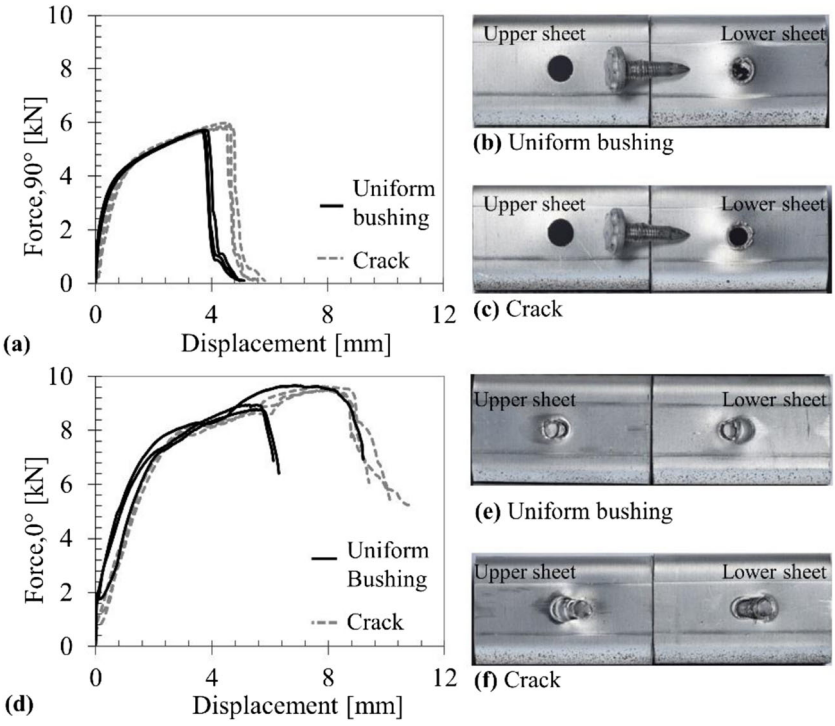

Fig. 13 Force–displacement curves obtained with the KS-II samples (**a**) at 90° (tensile) and (**d**) at 0° (shear) for the assembly aluminum 5182-O 2.5 mm (pre-hole)/aluminum 5182-O 2.5 mm. Assembly tested with the uniform bushing and with the cracked bushing. For the three tests with KS-II sample at 90° (tensile), the failure mode observed was (**b**) uniform bushing and (**c**) crack forming. For the three tests with KS-II sample at 0° (shear), the failure mode observed was (**e**) uniform bushing and (**f**) crack forming

Table 3 Coefficients used for time (s) and total energy (J) estimation by Eq. (3) with F_z, feed force (kN) and ω, rotation speed (10^3 rad/s)

Variable	a_0	a_1	a_2
Time	1.47	− 2.49	− 0.82
Energy	197.4	197.4	− 0.2

interpolation, which was attempted with the nth order complete polynomial

$$X(F_z, \omega) = \sum_{i=0}^{n} \sum_{j=0}^{i} b_{ij} F^{i-j} \omega^{j}. \quad (4)$$

Table 3 shows the coefficients identified for a power law fitting the penetration time (3 mm screw stroke) depending on the speed of rotation and the axial force, as well as the total energy. An inverse relationship between time and process control parameters, force, and rotational speed is predicted by the negative coefficients a_1 and a_2 found for the power law. The coefficients corresponding to the polynomial fitting the experimental torque and work rate values are given in Table 4.

The interpolation models fitted the entire set of data well, as illustrated in Fig. 14. Consequently, they allowed for a continuous representation of the experimental values of the process time, torque, energy, and work rate over the feasible drilling domain shown in Fig. 9a. These distributions are shown in Fig. 15.

This figure provides a quantitative overview of the impact of the parameters on the process outcome. Clearly, shorter process cycles require both large rotation speed and feed forces. Cycle time is a critical industrial driver; according to the results, its improvement requires more powerful equipment. However, this increase in power does not induce an increase in either torque or energy; thus, it does not have technical drawbacks and it is economically efficient, apart from the initial investment and the ability to reduce the rotation speed when the thread forming step starts. In turn, less powerful equipment leads not only to longer cycle times but also to higher energy consumption. However, robust process windows for good assembly conditions are available, whatever the available power.

In contrast, the value of the penetration torque has a very different trend, and it seems to provide an indicator of defect occurrence. Indeed, chip formation occurred for low torque values (less than 1.7…2 Nm). For torque values larger than 2.5 Nm, cracks developed in the bushing. Thus it seems that torque values between these two limits could be a good candidate for the on-line monitoring of the absence of process defects. No other such candidate indicator could be identified during this investigation. In addition, since the torque is carried by the screw, this result indicates that relatively universal screws may be used with any equipment in order to join the same materials.

Figure 15 also provides useful information for the physical interpretation of the defect occurrence. For low values of rotational speed and feed force (point (d) in Fig. 10), the friction dissipation power is low and thus the temperature rise in the drill zone is slow. However, because of the low value of the feed force, the temperature in the drill zone finally reaches high values before complete piercing, so the material becomes ductile enough to avoid cracks. In turn, the drill time is very long. For high values of both rotation speed and feed force, (point (f) in Fig. 10), the friction power is high. The temperature rise is fast and the drilling occurs at a high temperature in spite of the high value of the feed force. Thanks to the elevated friction power, the drilling time is short. At point (h) of Fig. 10, the high feed force makes the screw pierce the sheet at lower temperature, the temperature rise being slower because of the low friction dissipation power. Thus cracks occur in this configuration.

For DP600, the bushing cracks are probably due to an insufficient ductility of the material during the drilling, as in the case of AA5182-O. Because the DP600 resistance is higher than that of AA5182-O, the temperature that needs to be reached in the drill zone for the screw to pierce the sheet is higher. However, this temperature rise is limited by the heat transfer to the screw tip. The temperature rise within the screw is greater in the case of DP600 because of the higher temperature required to pierce the sheet, and also because of the much lower thermal diffusivity of the steel. The thermal diffusivity governs the heat repartition between the screw and the sheet. The failure of the screw occurs at the beginning of the

Table 4 Coefficients used for the torque (Nm) and power (W) estimation by the 4th order polynomial law Eq. (4) with F_z, feed force (kN) and ω, rotation speed (10^3 rad/s)

Variable	b_{00}	b_{10}	b_{11}	b_{20}	b_{21}	b_{22}	b_{30}	b_{31}	b_{32}	b_{33}	b_{40}	b_{41}	b_{42}	b_{43}	b_{44}
Torque	− 0.68	− 0.09	2.49	2.45	− 0.23	− 1.21	− 0.55	− 0.05	0.04	0.24	− 0.12	− 0.10	0.05	− 0.01	− 0.02
Power	− 39.14	0.80	− 115.1	448.9	19.15	131s.0	− 128.8	0.65	1.17	− 17.1	− 27.05	− 6.37	0.75	0.06	0

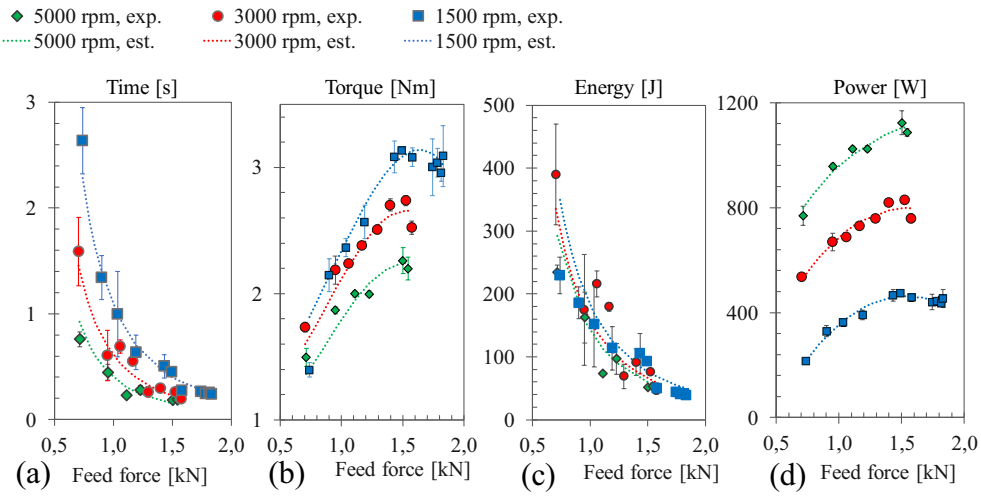

Fig. 14 Time and torque experimental values and interpolation curves with respect to the feed force, for three ranges of rotation speed at 3 mm

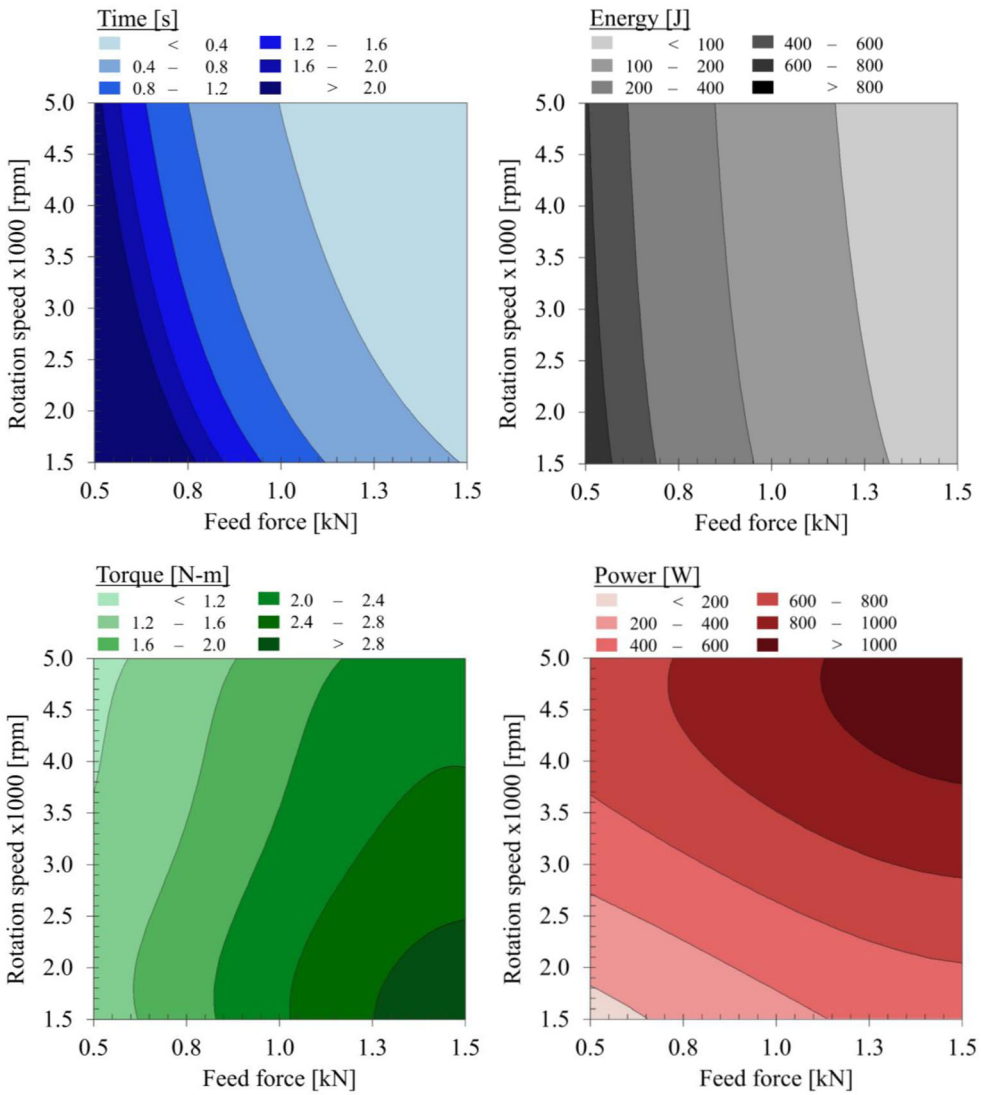

Fig. 15 Experimental variation of the time, total energy, torque, and power at 3 mm (end of penetrating stage) over the entire process window, for the 2.5 mm thick AA5182-O sheet aluminum alloy

sheet piercing by the tip of the screw. This position of the screw is associated with a quick increase of the torque (see Fig. 5). The piercing of the sheet and the hole formation are critical stages for the resistance of the screw.

5 Conclusions

An extensive experimental investigation allowed for the identification of flow drill screw driving defects during the drilling phase for two materials typical for automotive applications. A direct link was observed between the defect occurrence and the values of the two process driving parameters. Consequently, it is possible to modify the local conditions (heating/softening) in order to improve the material ductility and avoid defect occurrence.

The bushing crack defects occurred for both the sheet aluminum alloy and the sheet steel, for combinations of large feed force and low rotation speed. This defect did not affect the static resistance of the joint. The high strength steel led to the failure of the screw in a large area of the available process window.

The output parameters like the torque, process time, total energy, and maximum energy rate consistently depend on the driving parameters. The shortest cycle time corresponds to a large energy rate, but low total energy. The value of the drilling torque seemed to correlate well with the occurrence of the observed defects: chips for low torque values and cracks for large values. Consequently, such global process parameters may serve for flawless process monitoring during industrial application.

Funding information This work was supported by IRT M2P (Institut de Recherche Technologique Matériaux, Métallurgie et Procédés), the French PIA (Plan d'Investissement d'Avenir), and a consortium of industrial partners through projects SAM and PIRAMID.

Compliance with ethical standards

Conflict of interest The authors declare that they have no conflict of interest.

References

1. Martinsen K, Hu SJ, Carlson BE (2015) Joining of dissimilar materials. CIRP Ann Manuf Technol 64(2):679–699
2. Meschut G, Janzen V, Olfermann T (2014) Innovative and highly productive joining technologies for multi-material lightweight car body structures. J Mater Eng Perform 23(5):1515–1523
3. Miller SF, Blau PJ, Shih AJ (2005) Microstructural alterations associated with friction drilling of steel, aluminum, and titanium. J Mater Eng Perform 14(5):647–653
4. Fromentin G, Bierla A, Minfray C, Poulachon G (2010) An experimental study on the effects of lubrication in form tapping. Tribol Int 43(9):1726–1734
5. Urbikain G, Perez JM, López de Lacalle LN, Andueza A (2018) Combination of friction drilling and form tapping processes on dissimilar materials for making nutless joints. Proc Inst Mech Eng B J Eng Manuf 232(6):1007–1020
6. Skovron JD, Prasad RR, Ulutan D, Bo B, Paolini D, Mears L, Claus L, Detwiler D (2015) Effect of thermal assistance on the joint quality of Al6063-T5A during flow drill screwdriving. J Manuf Sci Eng 137(5):051019
7. Streppel AH, Kals HJJ (1983) Flowdrilling : a preliminary analysis of a new bush-making operation. CIRP Ann Manuf Technol 32(1): 167–171
8. Zimmer S, Langlois L, Laye J, Bigot R (2010) Experimental investigation of the influence of the FSW plunge processing parameters on the maximum generated force and torque. Int J Adv Manuf Technol 47(1-4):201–215
9. Markov OE, Perig EV, Markova MA, Zlygoriev VN (2016) Development of a new process for forging plates using intensive plastic deformation. Int J Adv Manuf Technol 83(9-12):2159–2174
10. Miller SF, Tao J, Shih AJ (2006) Friction drilling of cast metals. Int J Mach Tools Manuf 46(12–13):1526–1535
11. Lee SM, Chow HM, Huang FY, Yan BH (2009) Friction drilling of austenitic stainless steel by uncoated and PVD AlCrN- and TiAlN-coated tungsten carbide tools. Int J Mach Tools Manuf 49(1):81–88
12. Miller SF, Li R, Wang H, Shih AJ (2006) Experimental and Numerical Analysis of the Friction Drilling Process. J Manuf Sci Eng 128(3):802
13. Qu J, Blau PJ (2008) A new model to calculate friction coefficients and shear stresses in thermal drilling. J Manuf Sci Eng 130(1): 014502
14. Skovron J, Mears L, Ulutan D, Baeumler B, Paolini D, Claus L, Detwiler D (2014) Characterization of flow drill screwdriving process parameters on joint quality. SAE Int J Mater Manuf 8(1):35–44
15. Chow HM, Lee SM, Yang LD (2008) Machining characteristic study of friction drilling on AISI 304 stainless steel. JMPT 207(1–3):180–186
16. Sønstabø JK, Holmstrom PH, Morin D, Langseth M (2015) Macroscopic strength and failure properties of flow-drill screw connections. J Mater Process Technol 222:1–12
17. Kerkhofsa M, Van Stappena M, Quaeyhaegensb C, Stals LM (1994) The performance of (Ti , A1) N-coated flowdrills. Surf Coat Technol 68(1):741–746
18. Grossberndt, Hermann, Gunter Kretschmer, and Horst Klees. (1993) Hole forming and selftapping screw. U.S. Patent No. 5, 234,301. 10 Aug. 1993
19. Aslan F, Langlois L, Mangin P, Balan T (2018) Identification of drilling parameters during the flow drill screw driving process. Key Eng Mater 767:465–471
20. Szlosarek R, Karall T, No E, Hahne C, Meyer N (2013) Mechanical testing of flow drill screw joints between fibre-reinforced plastics and metals. Mater Test 55(10):737–742
21. Jawahir IS, Oxley PLB (1988) The tool restricted contact effect as a major influencing factor in chip breaking: an experimental analysis. CIRP Ann Manuf Technol 37(1):121–126
22. Kim TH, Yum J, Hu SJ, Spicer JP, Abell JA (2011) Process robustness of single lap ultrasonic welding of thin, dissimilar materials. CIRP Ann Manuf Technol 60(1):17–20
23. Sønstabø JK, Morin D, Langseth M (2018) Testing and modelling of flow-drill screw connections under quasi-static loadings. J Mater Process Technol 255(7491):724–738